Effect of the small-scale auxiliary laser spots on the $3\omega_0/2$ harmonic emission

Zunqi Lin, Huihuang Zhang, Xingfa He, Kangchun Lin, Xiaoqin Wang, Yifei Zhuang, Liushui Wang, Xiaochun Wei, Qirong Lu, Aing Shi, Meilan Dai, Li Tian, and Genliang Fan
High Power Laser and Physics Joint Laboratory, Shanghai Institute of Optics and Fine Mechanics, Academia Sinica, Shanghai, China

Jiaming Li
Institute of Physics, Academia Sinica, Beijing, China
(Received 29 October 1991)

Experiments have shown that a single 10-μm-radius laser spot is not able to produce the 90° side-emitted $\frac{3}{2}$ harmonic efficiently in a preformed laser plasma. However, with the help of one or two auxiliary laser spots with a size similar to that of the main spot, the side-emitted $\frac{3}{2}$ harmonic can frequently be detected when some positional and angular conditions for the auxiliary spots are met. The origin of these phenomena has been analyzed in terms of a proposed reflected laser photon-coupling model.

PACS number(s): 52.35.−g, 52.25.−b, 52.40.Nk, 42.25.Bs

I. INTRODUCTION

The $3\omega_0/2$ harmonic emission in a laser-plasma corona area originates from a two-step wave-interaction process [1–3]. In the first step an incident laser photon decays into two Langmuir plasmons with nearly equal frequency $\sim\omega_0/2$ at the $n_c/4$ density area when a threshold condition is satisfied. In the second step one of the decayed plasmons is coupled during its propagation phase with an incident or reflected laser photon, resulting in the generation of the $3\omega_0/2$ photon, when both the frequency and the wave-vector matching conditions are met. In principle, the second step can take place only around the $n_c/4$ density area of bulk plasma. This is because serious Landau damping may occur for the $\omega_0/2$ plasmons traveling downstream into a low-density region with a fast enhancement of plasma wave vectors. However, experiments [4] revealed that the $3\omega_0/2$ emission can extend spatially into a density as low as $n_c/20$.

Some authors ascribe the $3\omega_0/2$ in those low-density areas as coming from the $3\omega_0/2$ scattering by an ion acoustic wave which may be stimulated simultaneously in low-density areas [5,6]. The side-scattered $3\omega_0/2$ experimental observation showed [6] that the $3\omega_0/2$ signal decreases about 100 times while the electron density of bulk plasma decreases from $n_c/4$ to $n_c/20$. This fact may strengthen this proposal for the scattering mechanism. However, the $3\omega_0/2$ signal distribution along the density gradient is less variant within $n_c/4-n_c/10$, resulting in some uncertainty of the proposed mechanism.

To explain the extension of the $3\omega_0/2$ signal to an overdense area from the $n_c/4$, Short *et al.* [7] proposed a stable filamentation model under which a new $n_c/4$ layer may appear in a stable filament channel in a dense bulk-plasma environment. This model gave some explanation of the angle distribution of the $3\omega_0/2$ emission.

We proposed previously an unstable dynamic filamentation model [8,9] to meet the $3\omega_0/2$ emission properties of both spatial filamentation and temporal pulsation in an underdense plasma region. Recently, an image relay irradiation technique was developed to explore the details of the $3\omega_0/2$ feature in space and time [10]. An experiment for investigating the effect of many 10-μm-scale-laser spots on the $3\omega_0/2$ emission has revealed some unexpected properties. The experiment discovered a close relation of the side-emitted $3\omega_0/2$ signals with both the spot gaps and their angular orientations. Some interesting effects obtained were difficult to explain by the scattering model described above. A "reflected laser photon-coupling" model has been proposed to explain these observations.

II. EXPERIMENTAL ARRANGEMENT AND RESULTS

The image relay irradiation technique for target shooting has previously been described [10]. The prepulse beam with 1.06-μm wavelength and 250-ps pulse width, one beam of the Six Beam Laser Facility at High Power Laser and Physics Lab, SIOM, irradiated a polished Cu plane target at an irradiance of $(5-13)\times10^{12}$ W/cm^2 with a large spot 220 μm diameter. Another beam from the six was chosen as the main beam which was 500 ps delayed to the prepulse peak time for all shots in our experiment. The main beam produced an irradiance of $(3-8)\times10^{13}$ W/cm^2 on the target surface, which was adjusted at a prearranged image plane according to the image relay requirement. The polarization of the main beam was perpendicular to that of the prepulse, along the y and z directions in Fig. 1, respectively. By a polarizer, both the main and the prepulse beam shared a common laser incident axis x. There was an adjustable mask in the main laser beam, 19.6 m away from the $f/1.5$ aspherical target lens with $f=90$ mm. The main spot and the auxiliary spots from the main beam were defined as the spot along the diagnostic axis and the surrounding spots, respectively. Both the main spot and selected auxiliary spots were located on the prearranged image position of the Cu target surface. Different configurations of the main spot and auxiliary spots along with the large prepulse spot are summarized in Figs. 1(b) and 1(c). Figure 1(a) gives the spot projection layout.

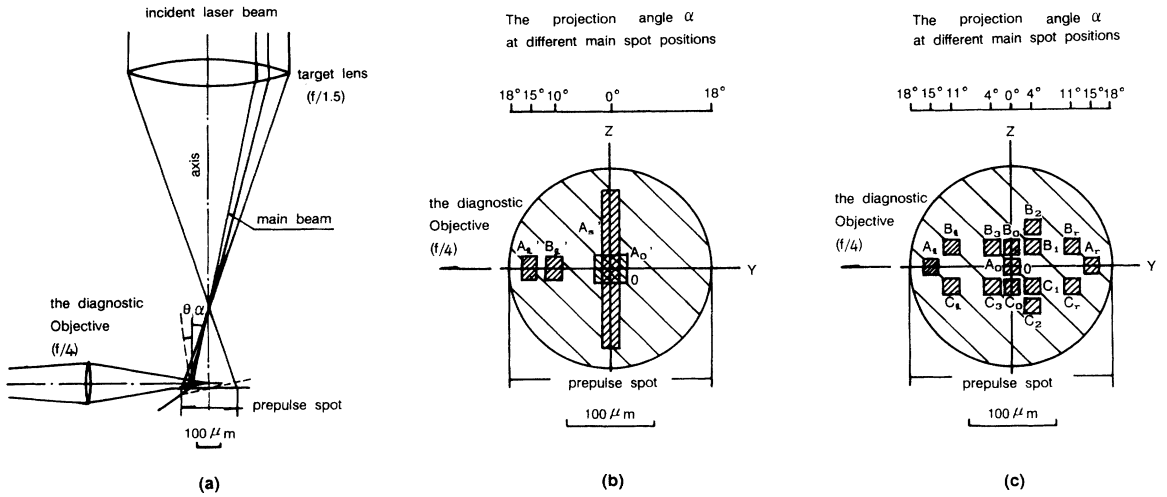

FIG. 1. All possible position arrangements of the image relay spots on the target surface for prepulse spots, main spots, and auxiliary spots. (a) Laser-beam projection creates a prepulse spot, main spots, and auxiliary spots by the image relay irradiation technique. The target surface is on the image plane of a mask, 19.2 m away from the aspherical target lens. α and θ represent the projection angle and the target-turning angle, respectively. (b) and (c) show the selectable main spots and auxiliary spots and their relative positions.

An optical streak camera with a time resolution of 30 ps viewed each type of the main spot side-on via an $f/4$ objective in a sampling window 150×5 μm along the incident main laser beam axis. The target surface positions in the window were marked on some shots. The magnification of the diagnostic optics was ~20.

Inserted in front of the streak camera slit was an interference filter with a central wavelength of 7100 Å, a

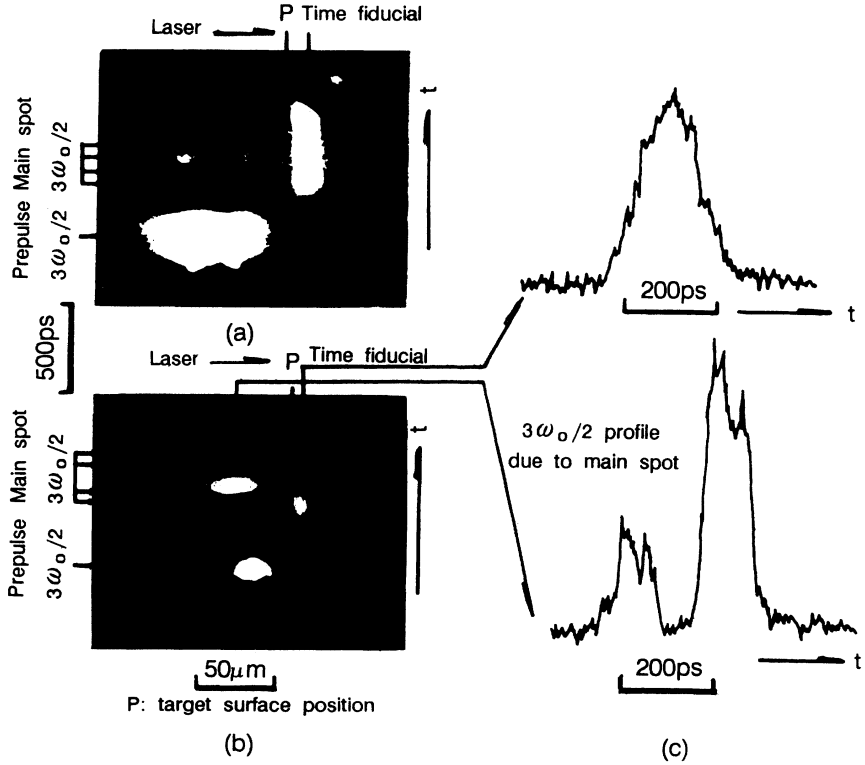

FIG. 2. (a) The photograph from shot No. 1. A polished Cu target was employed with $\theta=10°$, $A_0B_1C_1$ spot configuration, all of a size 18×18 μm^2, and the laser irradiance of 1.3×10^{13} and 8.8×10^{13} W/cm^2 for the prepulse and main (or auxiliary) pulse, respectively. (b) Shot No. 2. Employed was a polished Cu target with $\theta=0°$, A_s' narrow spot of 18×200 μm^2 and the laser irradiance of 0.96×10^{13} and 6.3×10^{13} W/cm^2 for prepulse and main pulse, respectively. (c) The densitometric trace of (b). The above smooth trace is the incident laser temporal profile and the one below shows an irregular pulsation structure on the temporal profile of the $3\omega_0/2$ signal.

pass band 150 Å, and a rejection ratio 10^{-4} for the inhibit wave band. An optical fiber collected frequency-doubled laser light which was used as a temporal fiducial.

The spatial resolution of both the target lens and the diagnostic objective was better than 10 μm, which insured the image relay quality of both the main and auxiliary spots, and the diagnostic sampling quality as well.

From Fig. 1(a) it is noted that the incident angle of the main spot is $\theta+\alpha$, with θ the incident angle of the main beam along the central axis and α the spot projection angle.

The side-scattered $3\omega_0/2$ signals have never been obtained with a single 20-μm-diam main spot, which was located at any positions of A_0 (18 shots), A_l (3 shots), or A_r (2 shots), shown in Fig. 1(c), and was 500 ps delayed from the prepulse, though an accurate alignment and focusing procedure was repeatedly taken and the spot irradiance increased to 8×10^{13} W/cm^2. In contrast to these results, it was found that the prepulse with a 212-μm-diam spot in those shots always brought about strong side-emitted three half signals, even though the prepulse irradiances were only $(0.5-1)\times10^{13}$ W/cm^2. When the main single spot diameter increased to 50 μm, the side $3\omega_0/2$ signal became detectable.

Previous experiments have shown that 10-μm-radius auxiliary spots gave no contribution to the side $3\omega_0/2$ emission from the main spot with the same diameter, when the distances between the main spot and the auxiliary spots were larger than 50 μm [10]. For the $3\omega_0/2$ generation there must be some direct interaction of narrow auxiliary beams with the main beam while the auxiliaries are distributed within a surrounding space, 10 to 50 μm away from the main spot beam axis. To investigate the details several spot configurations were selected.

With $A_0B_1C_1$ or $A_0B_0C_0$ configurations in Fig. 1(c), in which A_0 denotes an 18×18 μm^2 main spot and B_1,C_1,B_0,C_0 the same size auxiliary spots, five shots from nine obtained the $3\omega_0/2$ signals, with a strong temporal pulsation, as typically shown in Fig. 2(a). In this photograph four temporal pulses can be discerned with a maximum spatial extension of 70 μm.

In all nine shots the target surface was tilted towards the diagnostic optics at 10° and the auxiliary spots were 32 μm or less away from the main at the lateral or rear-lateral direction of the main spot corresponding to the diagnostic optics. If the auxiliary spots were moved 51 μm away from the main along the lateral or rear-lateral direction, such as those in configuration $A_0B_2C_2$ in Fig. 1(c), no $3\omega_0/2$ signals can be observed by the diagnostic optics. If they were moved around the main spot to the front-lateral direction, as in configuration $A_0B_3C_3$ in Fig. 1(c), no $3\omega_0/2$ signal response was found as well. For the above distance and angle effect of auxiliary spot arrangement, it is difficult to be explained by the $3\omega_0/2$

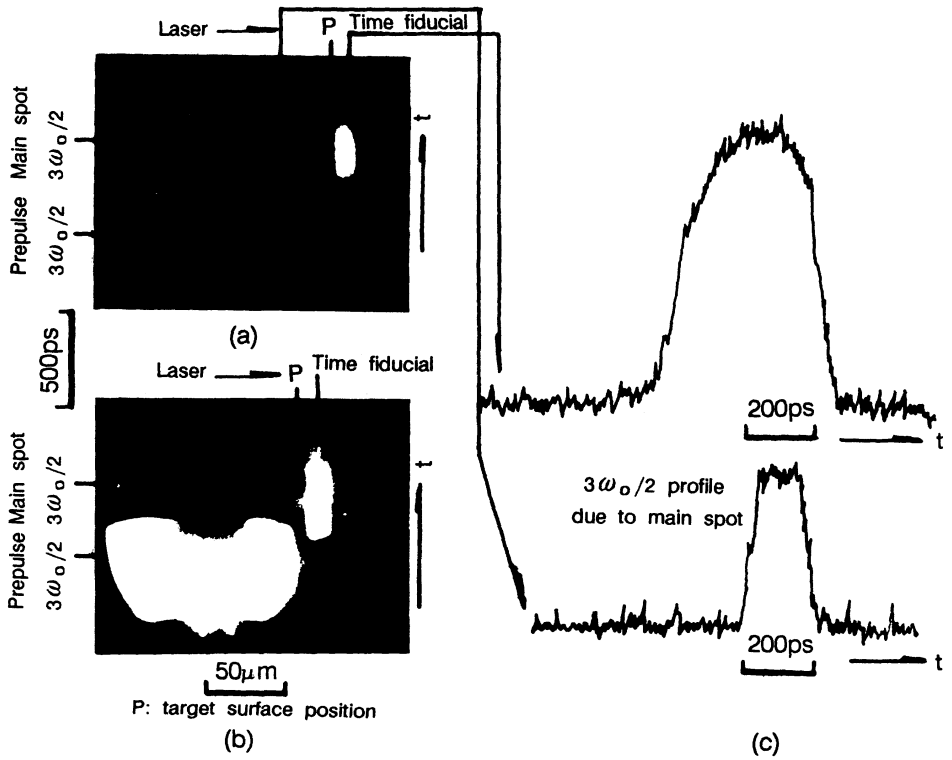

FIG. 3. (a) Shot No. 3. Employed was a polished Cu target with $\theta=10°$, $A_lB_lC_l$ spot configuration from Fig. 1(c), all of a size 18×18 μm^2 and the laser irradiance of 0.96×10^{13} and 6.3×10^{13} W/cm^2 for the prepulse and the main pulse, respectively. (b) Shot No. 4. Employed was a polished Cu target with $\theta=10°$, $A_rB_rC_r$ spot configuration from Fig. 1(c), all of a size 27×27 μm^2 and the laser irradiance of 1.2×10^{13} and 7.5×10^{13} W/cm^2 for the prepulse and the main pulse, respectively. (c) The densitometric traces of (a). The above trace shows the laser temporal profile which is broadened due to film saturation. The one below gives the temporal profile of the $3\omega_0/2$ signal which shows no serious modulation.

scattering mechanism, especially for the angle effect. According to the plasma wave scattering mechanism the three halves starting from the front-lateral-auxiliary spot should have been diffracted into the diagnostic optics.

As the main spot extended (along the z axis) to be an oblong spot A_s' with the vertical range larger than 50 μm, shown in Fig. 1(b), the $3\omega_0/2$ signal was able to be detected without adding any auxiliary spots. The signals were detected in 16 shots from a total of 23 shots in this case with θ varied from 0° to 20°. All of the measured three halves showed strong temporal pulsation. A typical photographic record is given in Fig. 2(b). The densitometric traces of the time fiducial and the three halves temporal evolution are plotted in Fig. 2(c). It is easy to observe a large difference between the smooth incident laser pulse and the serious harmonic modulation. It was found also that the pulsed feature of the $3\omega_0/2$ signal always appeared when the vertical range of A_s' increased from 50 μm to the maximum 220 μm.

By moving the main spot position to A_l and so the projection angle $\alpha=15°$, as shown in Fig. 1(c), the $3\omega_0/2$ signal was observed in five shots from the total of ten with $A_lB_lC_l$ configuration at target angle θ either 10° or 0°. It was found that the signal could be detected only at angle $\theta=10°$ in the above shots, resulting in the incident angle $\alpha+\theta=25°$ and 21°, for the light to spots A_l and B_l or C_l, respectively. In contrast to the previous results, the signal appeared to be smoothing in time. The spatial extension of the signal was also smaller than that of the previous results, as shown in Fig. 3(a). From the photo, the observed spatial extension resulting from the prepulse is 96 μm, in comparison with a 47-μm extension from the main pulse, inclinded to the left of the prepulse signal.

Figure 3(c) gives the densitometric trace of the laser time fiducial and the $3\omega_0/2$ signal for the main spot A_l. No serious modulation is obtained on either profiles.

Differing from the case of A_s', the $3\omega_0/2$ signal could not be detected in three shots when the spot A_l extends vertically to a range larger than 50 μm. This shows an incident angle effect on the $3\omega_0/2$ emission, which is also difficult to be understood by a plasma wave scattering mechanism.

By moving again the main spot position to A_r with projection angle $\alpha=15°$, but in an opposite inclination, the detected $3\omega_0/2$ signals in two shots became very weak with temporal pulsation while the spot configuration selected was $A_rB_rC_r$, shown in Fig. 1(c). Figure 3(b) gives an example of the shot.

By setting two spots A_l', B_l' on the x axis in Fig. 1(b) or by extending horizontally the spot A_0 to a range larger than 50 μm, the $3\omega_0/2$ signals detection became quite weak and fluctuated in four shots. Some weak $3\omega_0/2$ pulses were observed in two shots from the four, though the scattering theory predicted large scatter in a condition with both the signal source and plasma wave grating located on a diagnostic axis.

III. ANALYSIS AND DISCUSSION

We first review the scattering model which cannot explain our present experimental observation, then outline our proposed reflected laser photon coupling model and finally perform a phase-matching analysis for the $3\omega_0/2$ harmonic generations.

A. Scattering model

The scattering model ascribes the side-emitted $3\omega_0/2$ harmonic to scattering the $3\omega_0/2$ harmonic source from the auxiliary spots by plasma wave gratings generated simultaneously in the low-density region along the axis. The stimulated-Brillouin-scattering (SBS)-produced ion acoustic wave and the stimulated-Raman-scattering (SRS)-produced Langmuir wave can be the sources of the plasma wave gratings. By the scattering model it can be explained that the $3\omega_0/2$ emission can extend spatially into low-density regions. However, it is difficult to explain the following experimental observations by the scattering model: no $3\omega_0/2$ signals in both $A_0B_2C_2$ and $A_0B_3C_3$ spot configurations in contrast with clear $3\omega_0/2$ signals in the $A_0B_1C_1$ and $A_lB_lC_l$ spot configurations; weak $3\omega_0/2$ signals in $A_l'B_l'$ configuration in contrast with strong $3\omega_0/2$ signals in the $A_0B_0C_0$ configuration.

B. The reflected laser photon-coupling model

In our proposed model the side-emitted $3\omega_0/2$ harmonic is generated by coupling reflected laser photons ω_0 from the auxiliary spots with the $\omega_0/2$ plasmons induced by the local dynamical filamentation process in its transient phase. The dynamical filamentation process should be a complicated and unstable three-dimensional process owing to strong dynamical coupling between self-focusing and ponderomotive-force-induced electron-density modification in local small-scale filaments [11]. The relevant issue in our model is that the two-plasmon decay process (TPD) can occur in a fast-moving tip area of a dynamical filament [8,9]. The TPD-produced $\omega_0/2$ plasmons will be left at a transient filament wall, where the laser intensity drops down as the filament tip moves ahead quickly. The side-emitted $3\omega_0/2$ harmonic is produced by coupling the backreflected laser photons from the auxiliary spots with those dynamical-filamentation-induced $\omega_0/2$ plasmons. The detailed phase-matching analysis will be given later to illustrate the directions of the emitted $3\omega_0/2$ photons and to explain our present experimental observations of various spot configurations. The lifetime of the dynamical-filamentation-induced $\omega_0/2$ plasmons is quite short owing to very low environment density surrounding the transient filament wall. Therefore it leads to pulsation of the $3\omega_0/2$ emission. However, the $\omega_0/2$ plasmon lifetime becomes long as the surrounding environment density approaches $n_c/4$. This may be the case in the $A_lB_lC_l$ spot configuration shown in Fig. 1(c), in which the experimental result has shown the smooth $3\omega_0/2$ temporal behavior as displayed in Fig. 3(c) and indicates the $3\omega_0/2$ emission generated in the region with density about $n_c/4$.

The TPD process occurs in the tip area of the dynamical self-focusing filament which can be characterized by the following parameters α, β, and q [1–3]:

$$\alpha \equiv (4k_0|v_0|/\omega_0)k_0 L \ , \tag{1}$$

$$\beta \equiv 9v_e^4 k_0^2/|v_0|^2\omega_0^2, \tag{2}$$

$$q \equiv (k_y/k_0)^2 \ . \tag{3}$$

The k_0 denotes the local wave vector of the incident laser light, ω_0 the laser frequency, $v_0 = eE_0/(m_e\omega_0)$ the electron quivering velocity, L the linearized electron-density scale length with $n_e = n_0(1+x/L)$, $v_e = (k_B T_e/m_e)^{1/2}$ the electron thermal velocity, and k_y the y component of the $\omega_0/2$ plasma wave vector. From Eq. (2), $\beta = 1.41T^2/(I_{14}\lambda^2)$ where T is the electron temperature in keV, I_{14} is the laser intensity in the unit of 10^{14} W/cm^2, and λ the vacuum laser wavelength in μm. In the ponderomotive-force-induced self-focusing process in small scales, the laser intensity in the tip area of the filament increases rapidly while the electron temperature still keeps the value of the environment in a very short period. Taking into account 5–10 times enhancement of the laser irradiation of $(3-8)\times 10^{13}$ W/cm^2 in our experiment owing to the small-scale self-focusing, we can set I_{14} equal to about 3. T can be approximately equal to about 0.8, the upper-limit for the prepulse irradiance of $(5-12)\times 10^{12}$ W/cm^2 on the Cu target surface. Therefore, the upper-limit of β equals about 0.2 which is small indeed. The threshold conditions for the TPD process in the small-β (finite-βq) approximation, $3\alpha/(4\beta^{1/2}) > 3.094$ and $\beta q = 0.271$, lead to [3]

$$L\lambda I_{14}/T > 61.25 \ , \tag{4}$$

$$(k_y/k_0)^2 = 0.19(I_{14}\lambda^2/T^2) \ . \tag{5}$$

The L denotes the electron-density scale length in μm. From Eq. (4), $L_\mu > 16$ μm. From Eq. (5), k_y at least can be $0.94k_0$, which is two times more than the maximum k_y value of $0.4k_0$ [6], deduced from the bulk plasma case with a balanced I_{14} and T for the maximum growth rate.

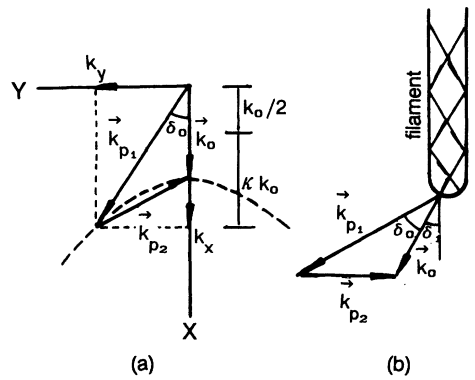

FIG. 4. (a) The wave-vector matching diagram in the TPD process. $\mathbf{K}_0$ is the laser wave vector. $\mathbf{K}_{p_1}$ and $\mathbf{K}_{p_2}$ are decayed plasmon wave vectors with the nearly equal frequency $\sim\omega_0/2$. k_x and k_y are the components on the x and y axis, respectively. $k_x \equiv k_0(\kappa + \frac{1}{2})$, δ_0 is defined as the angle between $\mathbf{K}_0$ and $\mathbf{K}_{p_1}$. (b) δ_1 is the angle clipped by $\mathbf{K}_0$ and the self-focusing filament axis, thus it describes a $\mathbf{K}_0$ angle variation caused by the deflection in a self-focusing process. $\delta_1 + \delta_0$ denotes the angle between $\mathbf{K}_{p_1}$ and the filament axis.

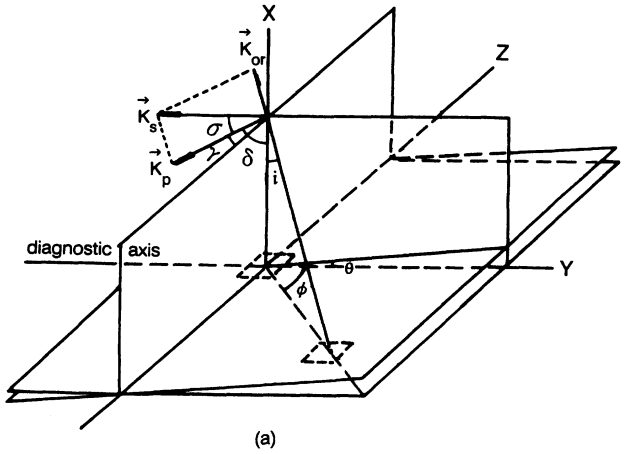

(a)

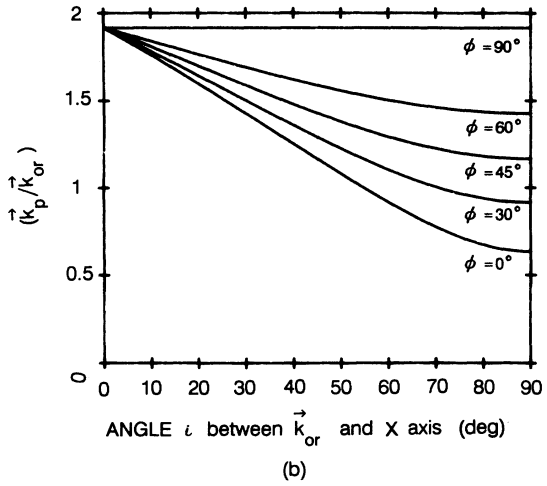

(b)

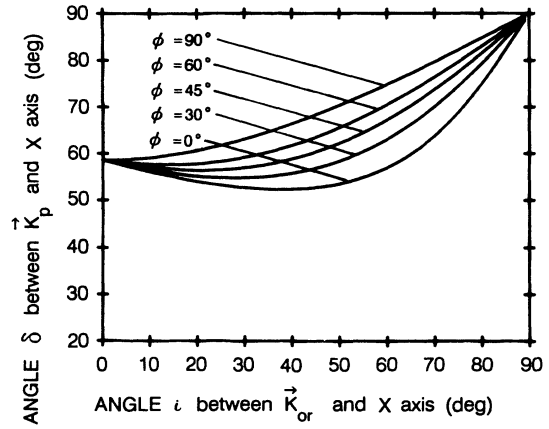

(c)

FIG. 5. (a) The wave-vector matching diagram for generation of the side-emitted $3\omega_0/2$ signal with a wave vector $\mathbf{K}_s$ in the $(-x)$ direction. $\mathbf{K}_{0r}$ denotes the wave vector of reflected light from an auxiliary spot with an angle i to the z axis and an angle ϕ to the x axis on the x-y plane. $\mathbf{K}_p$ denotes the $\omega_0/2$ plasmon wave vector generated at the main-spot-beam region with angles σ, γ, and δ to the y, z, and x axis, respectively. (b) $|\mathbf{K}_p|/|\mathbf{K}_{0r}|$ as a function of angle i in different parameter ϕ, the orientation of the auxiliary spot. (c) Required δ angle as a function of angle i in different parameters ϕ; δ represents the angle between $\mathbf{K}_p$ and the main-spot-beam axis.

Large k_y provides a suitable matching condition for generating 90° side-scattered three halves. The wave vectors of the $\omega_0/2$ Langmuir wave with the maximum growth rate can be fitted approximately as $k_x(k_x-k_0)=k_y^2$ as shown in Fig. 4. Thus, one has $k_x=1.56k_0$, $k_{p_1}=(k_x^2+k_y^2)^{1/2}=1.82k_0$. The angle δ_0 between $\mathbf{K}_0$ and $\mathbf{K}_{p_1}$ equals about 31°. Considering an angle δ_1 between $\mathbf{K}_0$ and the filament axis, the angle between $\mathbf{K}_{p_1}$ and the filament axis should become $\delta=\delta_0+\delta_1$, as shown in Fig. 4(b).

δ_1 can be large when the cross section of a filament channel becomes small enough. Furthermore, taking into account the depolarization effect in the filaments, we anticipate the wave vector $\mathbf{K}_{p_1}$ to appear in all orientations of polarization. This is consistent with the experimental observations which have been independent of the incident laser polarizations [4,9,10].

C. The phase-matching analysis

To analyze our experimental result, the vector matching diagram in the second coupling step is plotted in Fig. 5(a), where $\mathbf{K}_{0r}$, $\mathbf{K}_p$, and $\mathbf{K}_s$ denote the reflected light wave vector from the auxiliary spot, the $\omega_0/2$ plasmon wave vector, and the produced $3\omega_0/2$ harmonic wave vector in the diagnostic direction of $(-y)$, respectively. $\mathbf{K}_{0r}$ has an angle i with the x axis and its projection in the y-z plane has an angle ϕ with the y axis. $\mathbf{K}_p$ has the angle σ, γ, and δ with y, z, and x, respectively. From the vector matching geometry in our experimental condition, the $\mathbf{K}_p$ amplitude and its direction angle δ required can be deduced as

$$k_p=k_{0r}\left(\tfrac{11}{3}-4\sqrt{\tfrac{2}{3}}\sin i\cos\phi\right)^{1/2}, \tag{6}$$

$$\delta=\cos^{-1}\left[\left(\tfrac{11}{3}-4\sqrt{\tfrac{2}{3}}\sin i\cos\phi\right)^{-1/2}\cos i\right]. \tag{7}$$

The k_p/k_{0r} and δ, as a function of i in the different parameter ϕ, are plotted in Figs. 5(b) and 5(c), respectively. The required k_p, covering a range from $0.63k_{0r}$ to $1.91\,k_{0r}$, is well coincident with the previous estimation $k_{p_1}\cong 1.82k_0$, or $k_p\cong 1.82k_{0r}$. The range of angle i is limited at about 10°–30°, estimated by a large number of auxiliary spot position experiments. The angle δ may thus cover a range from 50° to 60°, an experimentally available turning angle range of $\mathbf{K}_p$.

When the $\omega_0/2$ plasmon Langmuir wave, originated by the beam self-focusing of the main spot [11], travels down to a low-density environment of bulk plasma, the wave vector will increase rapidly at its propagation phase with the fixed frequency. In addition, the transient nonuniform density distribution by self-focusing will make the wave-vector direction changed. Those changes make $\mathbf{K}_p$ more flexible to fit the wave-vector matching condition. Besides these, the small-scale self-focusing can also occur in auxiliary spots, resulting in a ray divergence of incident laser light and so the divergence of reflected photon vector. This effect makes $\mathbf{K}_{0r}$ more flexible for the vector matching, leading to the emission of the 90° side $3\omega_0/2$ signals from a broad space. It should be noted here that the temporal synchronization or the simultaneity factor of self-focusing between the main spot and the auxiliaries is an essential factor for the vector matching in a broad space. This factor may be the main cause of the $3\omega_0/2$ pulsation and nonreproducible behavior in the experimental observation.

The adjustment of target turning angle θ plays a role of reorientation of the reflected light from the auxiliary spots. A suitable adjustment of the angle θ can make a group of reflected rays with the optimum angles coupled to the $\omega_0/2$ plasmons at the main spot beam, resulting in a large possibility of the $3\omega_0/2$ production.

The target turning angle effect clearly appeared in group experiments at configuration $A_lB_lC_l$. With a target turning angle $\theta_0=10°$, simple geometrical deduction shows that the reflected light from the auxiliary spot will meet the main-spot beam at a position nearly 20 μm away from the n_c surface, which is just at or close to the area of the $n_c/4$ in the performed plasma [12]. The lifetime of the $\omega_0/2$ plasmon should be long at the $n_c/4$ area of the bulk-plasma environment, no matter how originated, owing to small Landau damping. As the reflected light travels directly into the $n_c/4$ area to couple with the long-lifetime plasmons, the temporal pulsation behavior of the $3\omega_0/2$ signal becomes less evident. With a normal target-turning angle $\theta_0=0°$, the $\mathbf{K}_{0r}$ of the reflected photon could not meet the angle matching condition for the $3\omega_0/2$ 90° side emission, resulting in failure of the signal detection in a total of five shots in our experiment. The target-turning angle experiment has given evidence that the reflected photons did take part in the coupling process for the $3\omega_0/2$ 90° side emission.

For the configuration $A_l'B_l'$ or horizontally extended A_0, the reflected light from B_l' or another auxiliary spot in the extended A_0 case may suffer from serious deflection by the transient filament wall. Therefore it could be difficult for the reflected light to cross the channel to arrive at the other side of a filament for proper coupling with the $\omega_0/2$ plasmons in order to produce the $3\omega_0/2$ side emission. This may be the reason for the very small detection possibility for the $3\omega_0/2$ signal obtained at this configuration. This effect will be investigated further in detail in the future.

IV. CONCLUSION

The behavior of the side-scattered $3\omega_0/2$ signal has been investigated by a group of small-scale spot experiments. The temporal pulsation, signal nonreproducibility, and other complicated phenomena may be explained by a proposed reflected laser photon-coupling model. The scattering model is also analyzed. This research may be beneficial to explore more details of small-scale self-focusing filamentation, which may be more important than our current understanding in laser-produced plasmas.

ACKNOWLEDGMENTS

The authors acknowledge the technical assistance from the staffs working at the Six Beam Laser Facility. This work was supported by Chinese National Nature Science Foundation Contract No. 69078038.

[1] C. S. Liu and M. N. Rosenbluth, Phys. Fluids **19**, 967 (1976).
[2] A. I. Avrov *et al.*, Zh. Eksp. Teor. Fiz. **72**, 970 (1977) [Sov. Phys. JETP **45**, 507 (1977)].
[3] A. Simon *et al.*, Phys. Fluids **26**, 3107 (1983).
[4] M. J. Herbst, J. A. Stamper, R. R. Whitlock, R. H. Lehmberg, and B. H. Ripin, Phys. Rev. Lett. **46**, 328 (1981).
[5] H. C. Barr and F. F. Chen, Phys. Fluids **30**, 1180 (1987).
[6] P. E. Young, B. F. Lasinski, W. L. Kruer, E. A. Williams, K. G. Estabrook, E. M. Campbell, and H. A. Baldis, Phys. Rev. Lett. **61**, 2766 (1988).
[7] R. W. Short, W. Seka, K. Tanaka, and E. A. Williams, Phys. Rev. Lett. **52**, 496 (1984).
[8] Zunqi Lin, Opt. Commun. **42**, 351 (1982).
[9] Z. Lin, W. Tan, M. Gu, G. Mei, C. Pan, W. Yu, and X. Deng, Laser Part. Beams **4**, 231 (1986).
[10] Z. Lin *et al.*, Acta Phys. Sin. **40**, 234 (1991).
[11] R. D. Jones, W. C. Mead, S. V. Coggeshall, C. H. Aldrich, J. L. Norton, G. D. Pollak, and J. M. Wallace, Phys. Fluids **31**, 1249 (1988).
[12] Zhang Huihuang, Lin Zunqi, Wang Xiaoqin, and Yu. Wenyan, Chin. J. Lasers **18**, 45 (1991).

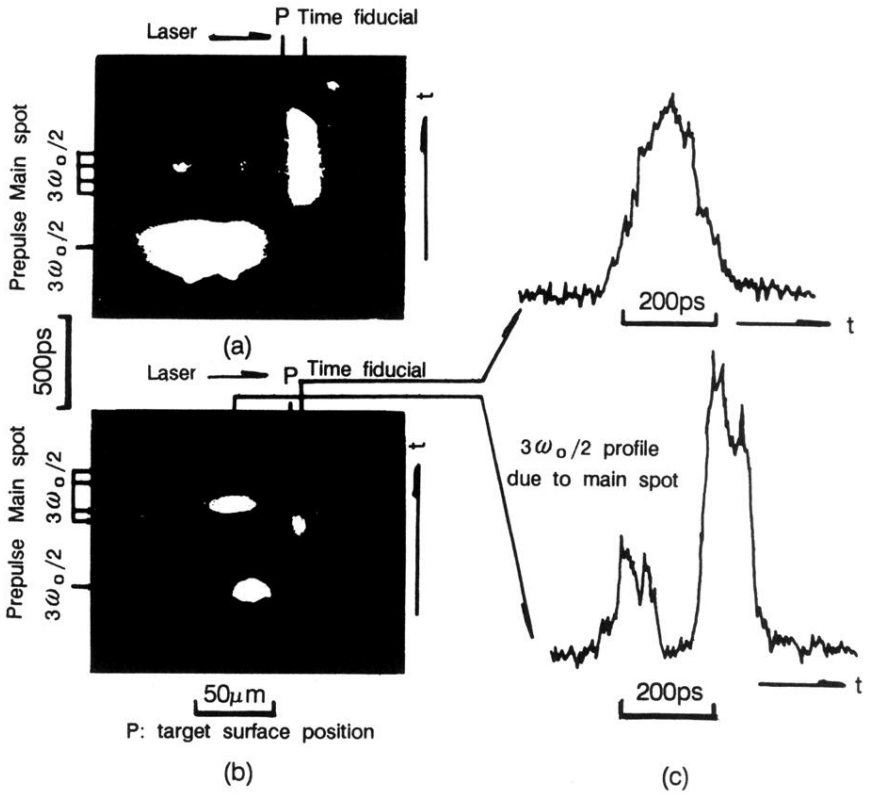

FIG. 2. (a) The photograph from shot No. 1. A polished Cu target was employed with $\theta=10°$, $A_0B_1C_1$ spot configuration, all of a size 18×18 μm^2, and the laser irradiance of 1.3×10^{13} and 8.8×10^{13} W/cm^2 for the prepulse and main (or auxiliary) pulse, respectively. (b) Shot No. 2. Employed was a polished Cu target with $\theta=0°$, A_s' narrow spot of 18×200 μm^2 and the laser irradiance of 0.96×10^{13} and 6.3×10^{13} W/cm^2 for prepulse and main pulse, respectively. (c) The densitometric trace of (b). The above smooth trace is the incident laser temporal profile and the one below shows an irregular pulsation structure on the temporal profile of the $3\omega_0/2$ signal.

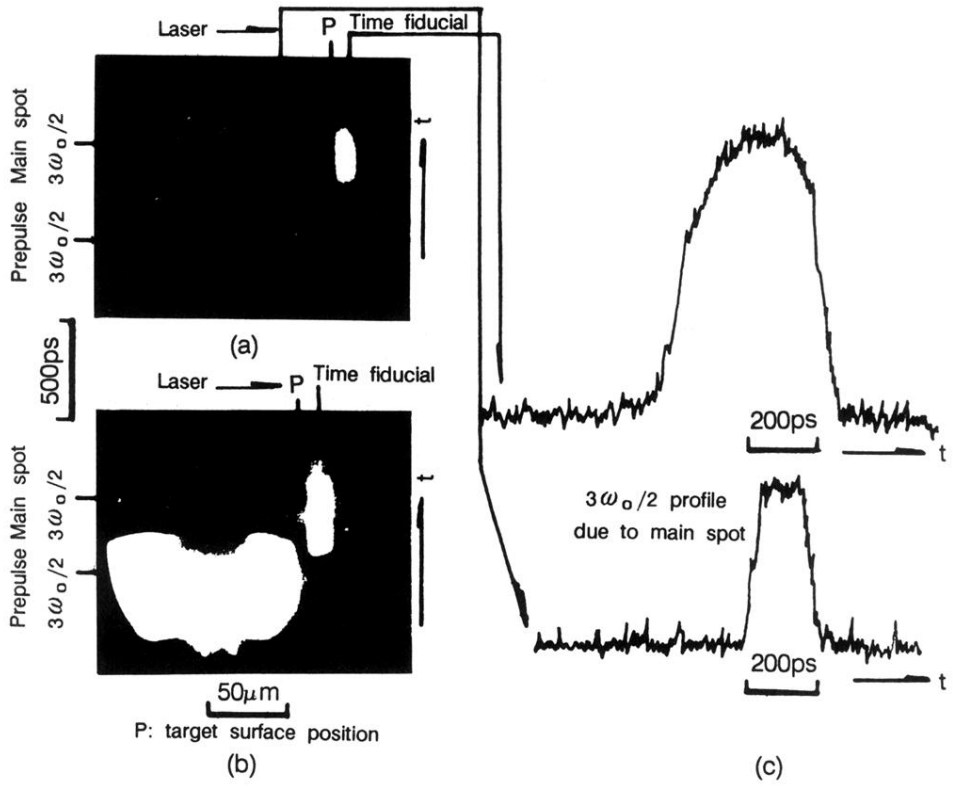

FIG. 3. (a) Shot No. 3. Employed was a polished Cu target with $\theta=10°$, $A_lB_lC_l$ spot configuration from Fig. 1(c), all of a size 18×18 μm^2 and the laser irradiance of 0.96×10^{13} and 6.3×10^{13} W/cm^2 for the prepulse and the main pulse, respectively. (b) Shot No. 4. Employed was a polished Cu target with $\theta=10°$, $A_rB_rC_r$ spot configuration from Fig. 1(c), all of a size 27×27 μm^2 and the laser irradiance of 1.2×10^{13} and 7.5×10^{13} W/cm^2 for the prepulse and the main pulse, respectively. (c) The densitometric traces of (a). The above trace shows the laser temporal profile which is broadened due to film saturation. The one below gives the temporal profile of the $3\omega_0/2$ signal which shows no serious modulation.